Pole-Zero Approach to Analyze and Model the Kink in Gain-Frequency Plot of GaN HEMTs

Sheikh Aamir Ahsan, *Graduate Student Member, IEEE*, Sudip Ghosh, *Member, IEEE*, Sourabh Khandelwal, *Member, IEEE*, and Yogesh Singh Chauhan, *Senior Member, IEEE*

***Abstract*—In this letter, we present a novel approach towards understanding the Kink-Effect (KE) in the Bode-plot of short circuit current gain (h_{21}) observed for microwave transistors, particularly GaN HEMTs. We ascribe the origin of the KE to the presence of a pair of complex conjugate poles at the frequency of interest, introduced due to the extrinsic parasitic inductances and their interaction with the device intrinsic elements such as the capacitances and transconductance, and develop simplified mathematical expressions that govern the behaviour of the kink. We also present a physics-based compact model that is capable of capturing the KE and extensively validate the model against measured data for a GaN device under multi-bias conditions, thereby advocating the strong physical background of the model. We conclude by demonstrating the impact of various elements of the small signal model on the kink based on the developed mathematical hypothesis for KE.**

***Index Terms*—Poles and zeros, GaN, h_{21}, kink-effect, model**

I. Introduction

GALLIUM Nitride (GaN) HEMTs are being widely researched for RF and microwave applications due to the phenomenal material properties of GaN such as wide bandgap, high electron saturation velocity etc [1], [2]. Kink-effects in the magnitude of the hybrid parameters of GaN HEMTs in the form of dips in h_{11} and h_{12} and peaks in h_{21} and h_{22} are observed, as shown in Fig. 1, similar to what was previously reported [3] for GaAs devices. Additionally, kink-effects in S_{22} have also been observed and modeled for GaN HEMTs [4], [5]. Here, we address the kink effect (KE) in the high frequency region of the Bode-plot of h_{21}, which is highly detrimental for the device microwave behavior and is known to impact high frequency figures of merit particularly the unity gain frequency (f_T). Crupi *et al.* attributed the KE to the phase cross-over of the open circuit output impedance (Z_{22}) [6]. In this manuscript, we essentially enhance that idea through an alternate approach i.e. by directly evaluating the expression for h_{21} and calculating the complex conjugate pair of poles to identify the resonant frequency. We further exploit the pole-zero approach to quantify the severity of the kink by deriving the mathematical expression for its conditional existence at the frequency where the complex conjugate pair of poles is located. It is done by computing the damping factor (ζ) in terms of the small signal model elements. Secondly, we present a physics-based compact model, as against look-up and table based models used in the previously reported works [6–8], to accurately predict the KE for GaN devices under a wide array of bias conditions, which is crucial from an RF circuit design perspective.

Manuscript received October 29, 2016; revised November 26, 2016; accepted December 12. Date of publication xxxxxxxx xx, 2017; date of current version xxxxxxx xx, 2017. This work was funded by Ramanujan fellowship research grant, Science and Engineering Research Board and Indian Space Research Organization.

S. A. Ahsan, S. Ghosh, and Y. S. Chauhan are with the Nanolab, Department of Electrical Engineering, Indian Institute of Technology Kanpur, India, 208016, e-mail: ahsan@iitk.ac.in, chauhan@iitk.ac.in

S. Khandelwal is with the Department of Electrical Engineering and Computer Science, University of California, Berkeley, USA.

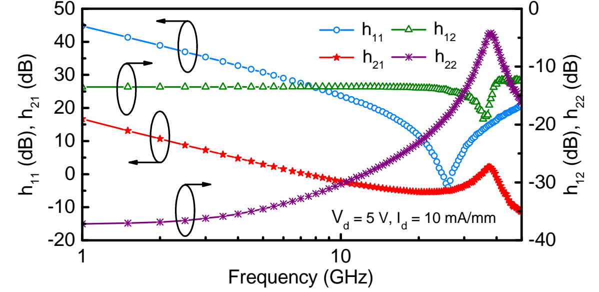

Fig. 1: Kink effects observed in magnitude of all the four hybrid parameters for a 10x90 μm GaN device, for $I_d = 10$ mA/mm. Dips in h_{11} and h_{12} and peaks in h_{21} and h_{22} are seen, similar to those previously reported for GaAs devices [3].

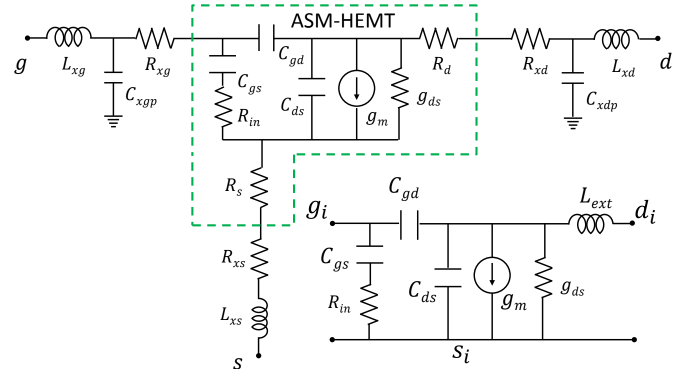

Fig. 2: Small Signal Equivalent Circuit (SSE) Model of the device. The dashed region represents the intrinsic device as described by the ASM-HEMT model. The capacitances, output conductance and the transconductance are calculated self-consistently from the surface potential [9]. Bias independent extrinsic elements are also shown. Also shown is simplified SSE of the intrinsic device without access region resistances [12], omitted only in our hand analysis to obtain easier parameter extraction, in conjuction with the effective extrinsic inductance L_{ext}.

II. Small Signal Model And Kink-Effect Theory

The small signal equivalent circuit (SSE) representation of the device is shown in Fig. 2. The elements within the dashed box represent the bias dependent intrinsic components of the device, governed by our surface-potential-based model named the ASM-HEMT Model, which is formulated in a Verilog-A code [9–11]. The bias-independent extrinsic parasitic elements are shown outside the dashed box. In Fig. 2, next to the overall device SSE, a simplified SSE is shown where we focus only on the capacitances (C_{gs}, C_{gd} and C_{ds}), the transconductance (g_m) and output conductance (g_{ds}) of the intrinsic device. L_{ext}, which represents the effective inductance presented by the source (L_{xs}) and drain (L_{xd}) inductances, is appended at the intrinsic drain node in order to realize the impact of the extrinsic inductive elements upon interaction with the intrinsic components. It must be noted that the access region

$$h_{21} = \frac{\frac{g_m}{C_{gd}} - s - s^2 R_{in} C_{gs}}{s\left[s^2 \left\{C_{eq} + R_{in} C_{gs}(g_{ds} + sC_{ds})\right\} L_{ext} + s\left\{R_{in}C_{gs} + \left(g_m + g_{ds}\left(1 + \frac{C_{gs}}{C_{gd}}\right)\right) L_{ext}\right\} + \left(1 + \frac{C_{gs}}{C_{gd}}\right)\right]} \tag{1}$$

resistances are included in the overall model simulation [10], [12], however omitted only in the hand analysis to avoid complicated and lengthier expressions for (1-7).

The h_{21} calculated for this SSE is given in (1), where $C_{eq} = C_{gs} + C_{ds} + \frac{C_{gs}C_{ds}}{C_{gd}}$. However, it is a point worthy to note that the non-quasistatic effects, which are captured by including a resistor R_{in} in series with C_{gs}, are generally observed at much higher frequencies (> 100 GHz) whereas the KE in h_{21} is seen at relatively lower frequencies ($\approx$ 50 GHz) [3], [14]. We can, therefore, reduce (1) by ignoring the contribution of R_{in} to obtain (2)

$$h_{21} = \frac{\frac{g_m}{C_{gd}} - s}{s\left[s^2 L_{ext} C_{eq} + s g_m^{'} L_{ext} + 1 + \frac{C_{gs}}{C_{gd}}\right]} \tag{2}$$

where $g_m^{'} = g_m + g_{ds}\left(1 + \frac{C_{gs}}{C_{gd}}\right)$. As can be seen, it is a single zero and 3-pole system with the zero z_1 located at $\omega = g_m/C_{gd}$ ($\approx 10^{12}$ rad/s) and one of the poles p_1 at ω = 0.

The locations of other two poles p_2 and p_3 are given as

$$p_{2,3} = \frac{-g_m^{'} L_{ext} \pm \sqrt{g_m^{'2} L_{ext}^2 - 4 L_{ext} C_{eq}\left(1 + \frac{C_{gs}}{C_{gd}}\right)}}{2 L_{ext} C_{eq}} \tag{3}$$

The term $g_m^{'2} L_{ext}^2$ in the square root is much smaller than the second term for a HEMT device, particularly in our case of extracted values of SSE elements, and hence can be ignored, leaving behind a much simpler expression for poles $p_{2,3}$ as

$$p_{2,3} \approx \pm j \sqrt{\frac{1 + \frac{C_{gs}}{C_{gd}}}{L_{ext}\left(C_{gs} + C_{ds} + \frac{C_{gs}C_{ds}}{C_{gd}}\right)}} \tag{4}$$

Since C_{gd} is generally much smaller than C_{gs} in saturation region, we can further simplify the expression as

$$p_{2,3} \approx \pm j \frac{1}{\sqrt{L_{ext}\left(C_{gd} + C_{ds}\right)}} \tag{5}$$

The above expression represents a pair of complex conjugate poles p_2 and p_3. It is this pair of poles which causes the emergence of a kink in h_{21} bode-plot. It happens when the damping ratio (ζ), which marks the boundary between complex (oscillatory motion) and real (exponential motion) roots, for this second order system becomes less than 0.5 [15], [16]. ζ can be obtained from (2) and the condition for emergence of kink can be written as

$$\zeta = \frac{g_m^{'}}{2} \frac{\sqrt{L_{ext}}}{\sqrt{\left(C_{gs} + C_{ds} + \frac{C_{gs}C_{ds}}{C_{gd}}\right)\left(1 + \frac{C_{gs}}{C_{gd}}\right)}} \leq 0.5 \tag{6}$$

We can simplify this condition by considering C_{gd} as a relatively smaller quantity in comparison to C_{gs}, given as

$$\zeta \approx \frac{\left\{g_m + g_{ds}\left(1 + \frac{C_{gs}}{C_{gd}}\right)\right\} C_{gd}}{2 C_{gs}} \sqrt{\frac{L_{ext}}{C_{ds}}} \leq 0.5 \tag{7}$$

This simplified expression for ζ gives an accurate behaviour followed by the kink, if the various model elements were to vary, as shown in the next section.

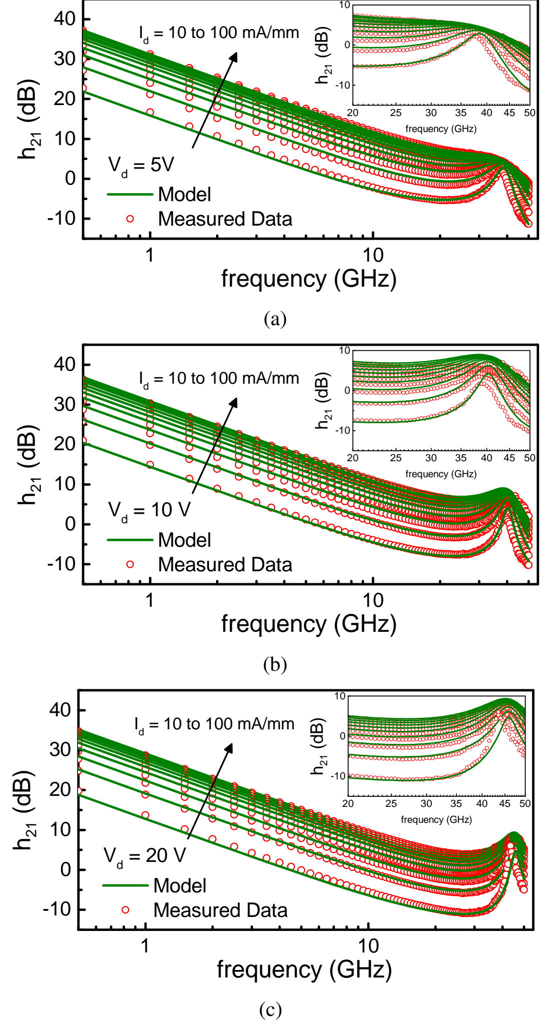

Fig. 3: Broadband Bode plots of h_{21} for a frequency range of 500 MHz to 50 GHz for a 10x90μm device. Three different V_d values (a) 5 V (b) 10 V (c) 20 V, each with ten V_g values. h_{21} drops at -20 dB/dec, before reaching the pair of complex poles, where kink is observed. The measured and modeled results are in excellent agreement.

III. Results and Discussion

We have implemented the model formulations in Verilog-A and performed simulations in Keysight's ADS circuit simulator. To start with, Fig. 3 shows an extensive comparison of the measured and modeled results for h_{21} of a 10x90 μm device for 30 different bias conditions - 3 different values of drain voltage V_d (5, 10 and 20 V) with 10 different values of gate voltage V_g (I_{ds} = 10 to 100 mA/mm) for each value of V_d. For each of the sub-plots, h_{21} starts off by falling at 20 dB/dec due to the pole $1/s$ at ω = 0, rises in the form of a kink as ω approaches the complex pair of poles $p_{2,3}$, and then upon extrapolating, further falls steeply at 60 dB/dec after having crossed $p_{2,3}$ [6]. The kink is observed to be severe for V_g values that result in low I_{ds}, which is understandable since low g_m reduces ζ and therefore a greater peaking as suggested by (7). The kink-frequency (f_k) increases with increasing V_d, which can be ascribed to reduced C_{gd}

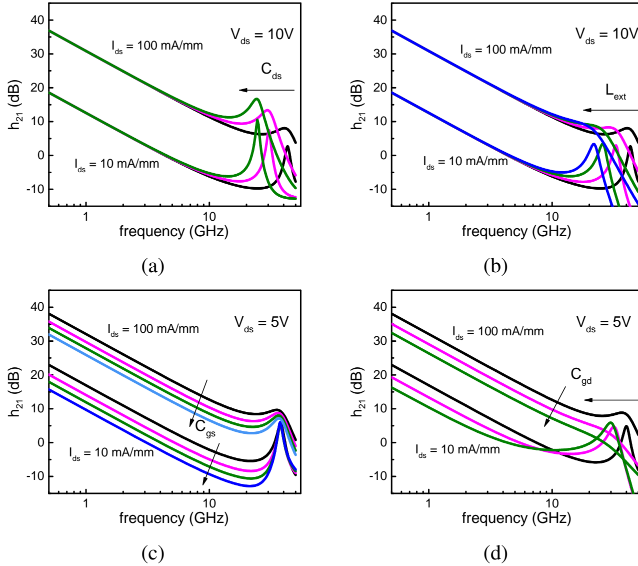

Fig. 4: Simulated h_{21} bode-plots highlighting the impact on the kink by individually varying (a) C_{ds}, (b) L_{ext}, (c) C_{gs} and (d) C_{gd}. The arrows indicate the direction of increasing values of model elements. The location of the kink as well as its severity is seen to be obeying trends in accordance with (5) and (7) respectively.

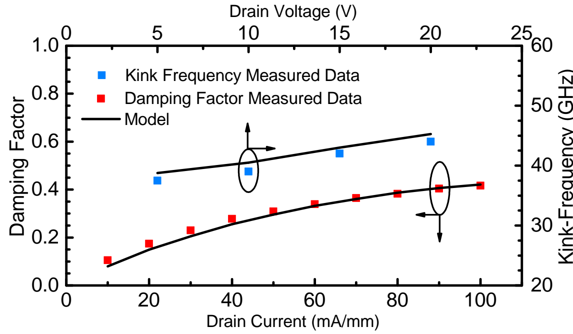

Fig. 5: Comparison of measured and modeled bias-dependence of kink-frequency (f_k) (for $I_d = 10\mathrm{mA/mm}$) and damping factor (ζ) (for $V_d = 5$ V), as functions of V_d and I_d respectively. Small signal elements extracted using methodology described in [13] are plugged in (5) and (7) to get f_k and ζ.

and C_{ds} with increasing V_d, causing $p_{2,3}$ to shift towards higher frequencies as governed by (5). Moreover, it is seen that for V_g values with higher I_{ds} the kink emerges before f_T which signifies the importance of modeling the KE in h_{21}. The accurate modeling of the kink effect with various bias conditions emphasizes the accuracy of bias dependence of the modeled device characteristics.

The impact of variation in various small signal model elements on the nature of the kink is highlighted in Fig. 4. The results are in accordance with (5) and (7). As is seen, the kink sharpens and shifts to lower frequencies as C_{ds} is increased. Increasing L_{ext} causes a similar effect as far as the shifting of the kink frequency is concerned, however, it causes a smoothing of the kink for high V_g values since it increases ζ and eventually pushes it beyond 0.5, whereas for low V_g values no smoothing of the kink is observed since low g_m is the dominant term in restricting ζ below 0.5. Increasing C_{gs} increases the prominence of kink as it reduces the overall gain as well as ζ, however C_{gs} variation has no impact on the location of the kink since the simplified expression for $p_{2,3}$ is independent of C_{gs}. C_{gd} variation effects the location of the kink as dictated by (5). An increase in C_{gd} smoothens the kink for high V_g values, which is obvious since it increases ζ but has little impact on the sharpness of the kink for low V_g values, where low g_m dominates the restriction in ζ.

Shown in Fig. 5 is a good quantitative agreement between the predicted and measured f_k and ζ variations with bias, obtained using (5) and (7). Parameter extraction methodology presented in [13] is used to extract the values of small signal elements that are plugged in (5) and (7). The model accurately captures f_k vs V_d and ζ vs I_d.

IV. Conclusion

We presented a pole-zero approach to understand the Kink-Effect in h_{21} for GaN HEMTs, which originates due to the existence of a complex pair of poles and the subsequent instability caused at the frequency of interest. We derived simplified mathematical expressions to calculate the location of the kink as well as the conditions that may lead to its severity. Additionally, we modeled this Kink-Effect using our physics-based compact model, and extensively validated the modeled results with multi-bias measured data. Lastly, an analysis was done to highlight as to how the kink responds to variations in different model elements or bias conditions.

References

[1] U. K. Mishra, *et al.*, "GaN-Based RF Power Devices and Amplifiers," *Proc. IEEE*, vol. 96, no. 2, pp. 287-305, Feb. 2008.

[2] R. S. Pengelly, *et al.*, "A Review of GaN on SiC High Electron-Mobility Power Transistors and MMICs," *IEEE Trans. Microw. Theory Techn.*, vol. 60, no. 6, pp. 1764-1783, Jun 2012.

[3] G. Crupi, *et al.*, "Identification of the intrinsic capacitive core for GaAs HEMTs by investigating the frequency behavior of the impedance parameters," *Microw. Opt. Technol. Lett.*, vol. 55, no. 6, pp. 1237-1240, Jun. 2013.

[4] S. A. Ahsan, *et al.*, "Modeling of Kink-Effect in RF Behaviour of GaN HEMTs using ASM-HEMT Model", *Proc. IEEE Conf. Electron Devices Solid-State Circuits (EDSSC)*, Hong Kong, Aug. 2016.

[5] G. Crupi, *et al.*, "Kink Effect in S22 for GaN and GaAs HEMTs," *IEEE Microwave Wireless Compon. Lett.*, vol 25, no. 5, pp 301303, May. 2015.

[6] G. Crupi, *et al.*, "A Clear-cut Understanding of the Current-Gain Peak in HEMTs: Theory and Experiments," *Microw. Opt. Technol. Lett.*, vol. 54, no. 12, pp. 2801-2806, Dec. 2012.

[7] G. Crupi, *et al.*, "An Extensive Experimental Analysis of the Kink Effects in S_{22} and h_{21} for a GaN HEMT," *IEEE Trans. Microw. Theory Techn.*, vol. 62, no. 3, pp. 513-520, Mar. 2014.

[8] A. Raffo, *et al.*, "Nonlinear dispersive modeling of electron devices oriented to GaN power amplifier design," *IEEE Trans. Microw. Theory Techn.*, vol. 58, no. 4, pp. 710-718, Apr. 2010.

[9] S. Khandelwal, *et al.*, "Analytical Modeling of Surface-Potential and Intrinsic Charges in AlGaN/GaN HEMT Devices," *IEEE Trans. Electron Devices*, vol. 59, no. 10, pp. 2856-2860, Oct. 2012.

[10] S. Khandelwal, *et al.*, "Robust Surface-Potential-Based Compact Model for GaN HEMT IC Design," *IEEE Trans. Electron Devices*, vol. 60, no. 10, pp. 3216-3222, Oct. 2013.

[11] S. A. Ahsan, *et al.*, "Capacitance Modeling in Dual Field-Plate Power GaN HEMT for Accurate Switching Behavior," *IEEE Trans. Electron Devices*, vol. 63, no. 2, pp. 565-572, Feb. 2016.

[12] S. Ghosh, *et al.*, "Modeling of Source/Drain Access Resistances and their Temperature Dependence in GaN HEMTs," *Proc. IEEE Conf. Electron Devices Solid-State Circuits (EDSSC)*, Hong Kong, Aug. 2016.

[13] S. Ahsan, *et al.*, "ASM-HEMT Model for RF and Power Electronic Applications - Overview and Extraction," *MOS-AK Workshop*, Shanghai, Jun. 2016.

[14] G. Crupi, *et al.*, "Investigation on the non-quasi-static effect implementation for millimeter-wave FET models," *Int. J. RF Microw. Computer Aided Eng.*, vol. 20, no 1, pp. 87-93, Jan. 2010.

[15] E. O. Doebelin, *Control System Principles and Design*, Ed. New York: John Wiley & Sons, 1985.

[16] M. Rao, and H. Qiu, *Process Control Engineering*, Gordon and Breach Science Publishers, 1993.